ACS APPLIED MATERIALS & INTERFACES

Research Article

www.acsami.org

Electrochemical Properties of ZrO_2-Doped V_2O_5 Amorphous Powders with Spherical Shape and Fine Size

You Na Ko,[†,‡] Seung Ho Choi,[†] Yun Chan Kang,*[,†] and Seung Bin Park[‡]

[†]Department of Chemical Engineering, Konkuk University, 1 Hwayang-dong, Gwangjin-gu, Seoul 143-701, Korea

[‡]Department of Chemical and Biomolecular Engineering, Korea Advanced Institute of Science and Technology, 291 Daehak-ro, Yuseong-gu, Daejeon 305-701, Korea

ABSTRACT: Amorphous V_2O_5 powders with zirconia (ZrO_2) dopant are prepared by one-pot spray pyrolysis at temperatures above the melting temperature of V_2O_5. The powders with 7 wt % ZrO_2 are completely spherical and dense with a clean surface, on which crystals of pure V_2O_5 powders are scarcely observed. The V_2O_5 powders with 7 wt % ZrO_2 have uniformly distributed V and Zr components. The uniformly distributed Zr component disturbs the crystallization of V_2O_5 during the quenching of the melted powders. These powders also give smooth initial discharge curves with a single slope, which is typical to amorphous materials. The discharge capacities of the V_2O_5 powders with 7 wt % ZrO_2 are 309, 269, and 222 mA h g^{-1} after the first, second, and 50th cycles, respectively, even at a high current density of 294 mA g^{-1}. The capacity retention measured after the first cycle is 83% after 50 cycles.

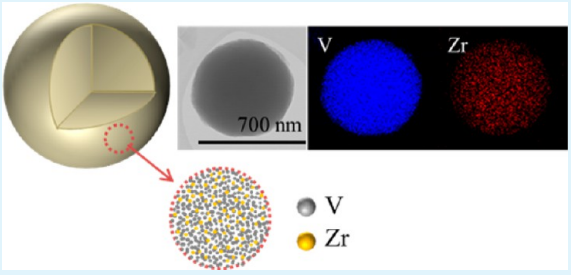

KEYWORDS: *Li-ion battery, cathode material, vanadium oxide, composite powders, amorphous material, spray pyrolysis*

1. INTRODUCTION

Vanadium pentoxide (V_2O_5) is one of the most promising cathode materials for Li-ion batteries because of its unique properties such as low cost and higher theoretical capacity as compared to typical cathode materials such as $LiCoO_2$.[1−11] When three Li ions are intercalated per mole of V_2O_5, the theoretical capacity reaches 440 mA h g^{-1}. However, the poor capacity retention of V_2O_5 remains a major problem, which results from the dissolution of V, damage of the crystal structure of V_2O_5, and the structural breakdown during the redox cycles.[12−16] To minimize the crystalline V_2O_5 shortcomings, researchers have widley investigated fine-sized V_2O_5 particles. Nanostructured V_2O_5 materials showed improved high rate performance because of their large surface to volume ratios and relatively short diffusion lengths.[10,11,17] But the major problems of the V_2O_5 could not sufficiently solved by just reducing the particle size.

Amorphous V_2O_5 has been investigated because of its interesting electrochemical performance.[18−25] In particular, the electrochemical properties of amorphous V_2O_5 aerogel, xerogel, and thin films prepared by complex methods have been studied. Coustier et al. showed that amorphous V_2O_5 with a large surface area prepared via a combined sol−gel and solvent exchange procedure shows very high Li insertion capacity and good capacity retention.[24] Amorphous V_2O_5 electrode with a protective thin film made of solid Li ion-conducting $LiAlF_4$ exhibited improved durability in terms of constant capacity even after repeated cycling up to 800 cycles.[25] Cathode powders with controlled morphology and submicrometer- or micrometer-sized particles can be applied in the commercial Li ion batteries. However, amorphous V_2O_5 powders with controlled morphology cannot be prepared by conventional liquid solution methods.

Spray pyrolysis has been employed to prepare spherical V_2O_5 cathode powders. Feng et al. prepared V_2O_5 cathode powders by spray pyrolysis at a low temperature (350 °C).[26] The crystalline V_2O_5 powders post-treated at 420 °C were spherical with a large surface area and high initial specific capacity of 399 mAh g^{-1}. Ko et al. showed that the crystalline V_2O_5 cathode powders directly prepared by spray pyrolysis have good electrochemical properties.[27] However, the electrochemical properties of amorphous V_2O_5 powders prepared by spray pyrolysis have not been studied.

In this study, amorphous V_2O_5 powders were prepared by one-pot spray pyrolysis at temperatures above the melting temperature of V_2O_5 (~690 °C). One amorphous V_2O_5 powder was formed from one droplet by drying, decomposition, melting, and quenching processes. The zirconia (ZrO_2) dopant disturbed the crystallization of the powder during quenching of the melted V_2O_5 powders. The effect of ZrO_2 on the crystal structure and electrochemical performance of the V_2O_5 cathode material prepared by one-pot spray pyrolysis was investigated.

2. EXPERIMENTAL METHODS

2.1. Material Synthesis. The spray pyrolysis system consisted of a droplet generator, a quartz reactor, and a Teflon bag filter (powder collector). A 1.7-MHz ultrasonic spray generator having six vibrators was used to generate a large amount of droplets, which were carried to

Received: January 20, 2013
Accepted: March 27, 2013
Published: March 27, 2013

   dx.doi.org/10.1021/am303150v | ACS Appl. Mater. Interfaces 2013, 5, 3234−3240

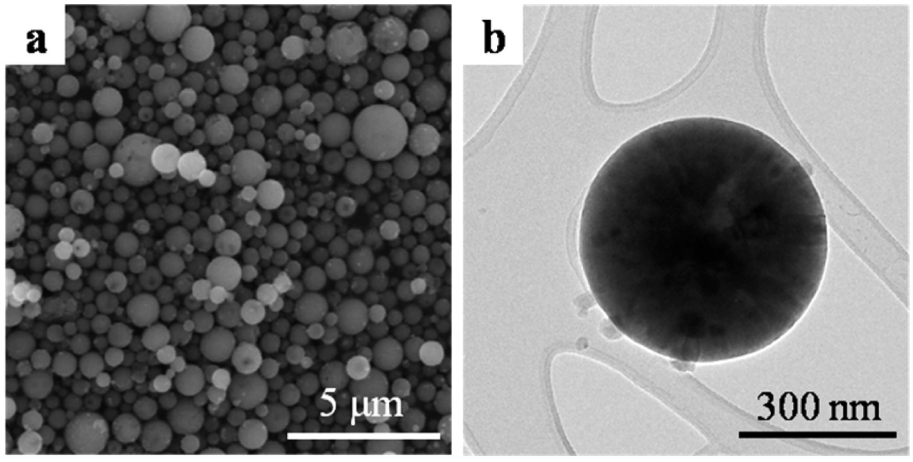

Figure 1. SEM and TEM images of the bare V_2O_5 powders prepared by spray pyrolysis at 1000 °C.

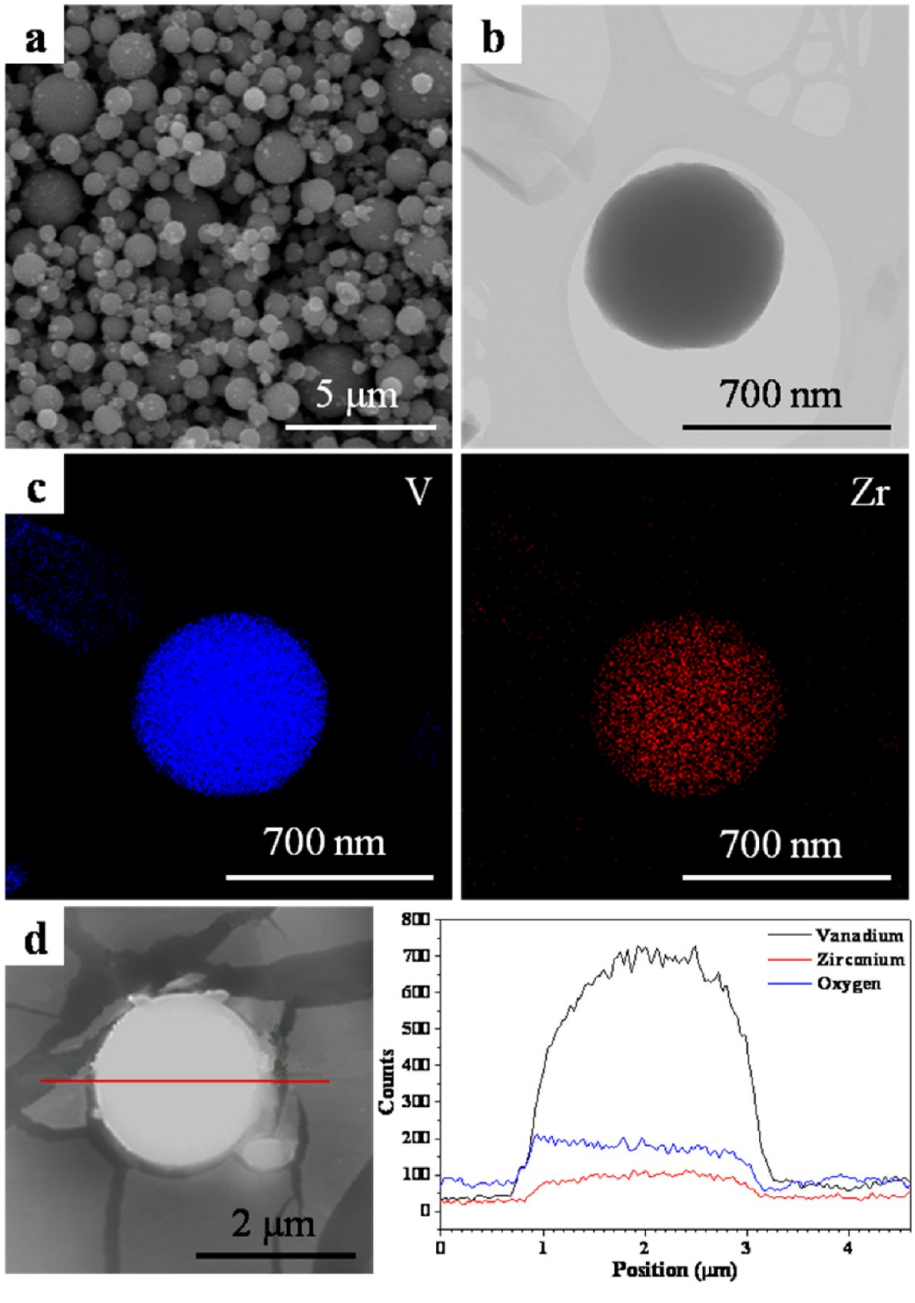

Figure 2. Morphologies, dot-mapping images, and the results of EDX line scan of the V_2O_5 powders with 7 wt % ZrO_2.

dx.doi.org/10.1021/am303150v | ACS Appl. Mater. Interfaces 2013, 5, 3234−3240

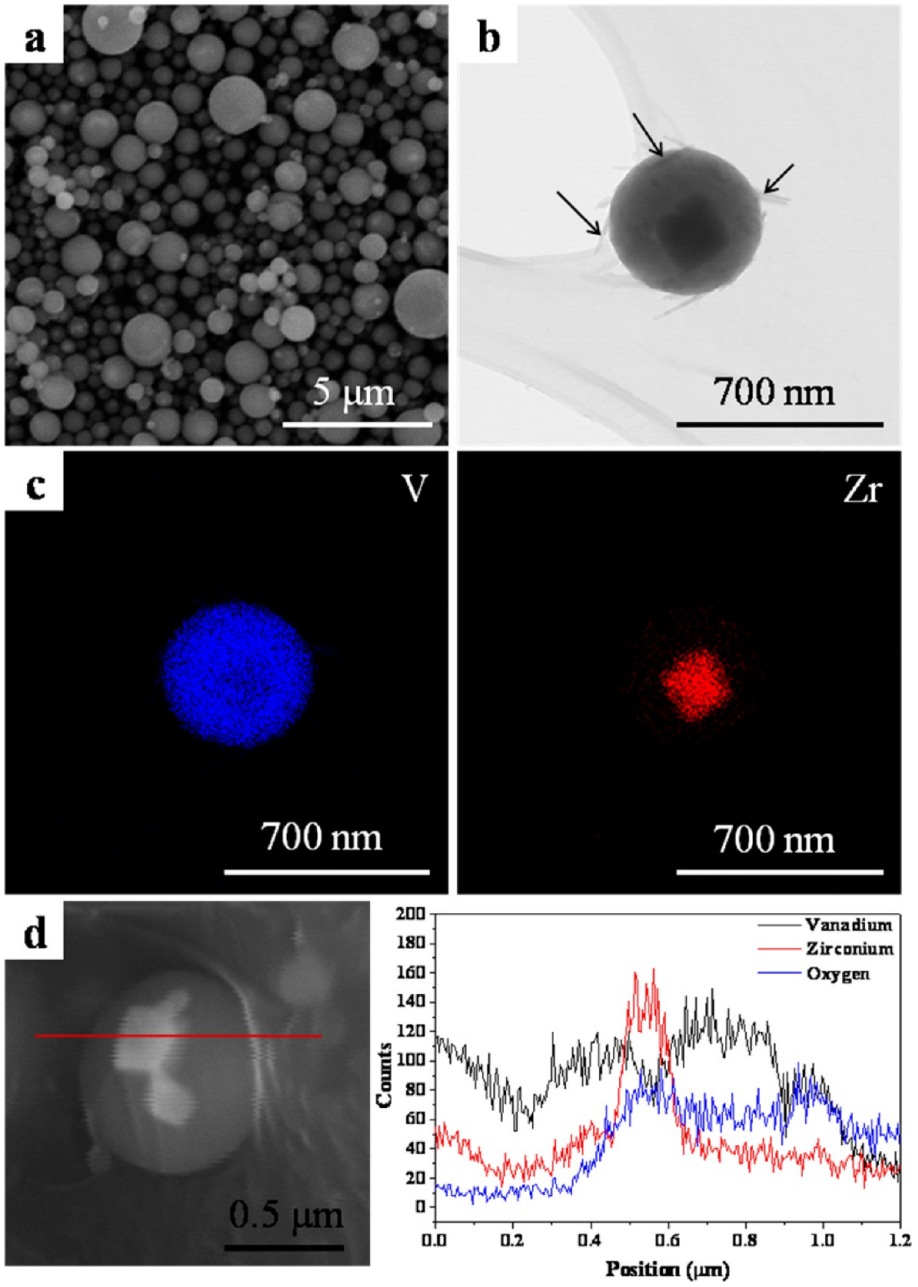

Figure 3. Morphologies, dot-mapping images, and the results of EDX line scan of the V_2O_5 powders with 15 wt % ZrO_2.

the high-temperature tubular quartz reactor by a carrier gas. The length and diameter of the quartz reactor were 1200 and 50 mm, respectively. The length of the single-zone heating furnace was 800 mm. The preparation temperature and the flow rate of air used as the carrier gas were fixed at 1000 °C and 10 L min^{-1}, respectively. The precursor solution was prepared by dissolving V_2O_5 and zirconyl nitrate hydrate in distilled water and nitric acid with heating. The total concentration of the V component was fixed at 0.08 M, and the doping concentration of ZrO_2 was changed from 0 to 15 wt % V_2O_5.

2.2. Characterizations. The morphologies of the V_2O_5 cathode powders with ZrO_2 additives were investigated by scanning electron microscopy (SEM, JEOL JSM-6060) and transmission electron microscopy (FE-TEM, JEOL-2100F). The crystal structures of the powders were investigated by X-ray diffractometry (XRD, X'Pert PRO MPD) using Cu Kα radiation (λ = 1.5418 Å)) at the Korea Basic Science Institute (Daegu). The XPS spectra of the V_2O_5 powders with ZrO_2 additives were investigated using X-ray photoelectron spectroscopy (XPS, ESCALAB-210) with Al Kα radiation (1486.6 eV). The binding energy was calibrated with reference to the C 1s level of carbon (284.6 eV). The elemental compositions of the V_2O_5 powders with ZrO_2 additives were investigated using an inductively coupled plasma−optical emission spectrometer (ICP-OES, Perkin-Elmer, OPTIMA 4300 DV).

The electrochemical properties of the prepared V_2O_5 powders were analyzed in a 2032-type coin cell. The cathode powder was prepared from a mixture of 20 mg composite powder and 12 mg TAB (TAB is a mixture of 9.6 mg teflonized acetylene black and 2.4 mg binder). Li metal and a microporous polypropylene film were used as the anode and the separator, respectively. The electrolyte was 1 M $LiPF_6$ in a 1:1 mixture (by volume) of ethylene carbonate/dimethyl carbonate (EC/DMC). The cells were tested in the 1.5−4.0 V range at a constant current density of 294 mA g^{-1}.

3. RESULTS AND DISCUSSION

Figure 1 shows the morphologies of V_2O_5 powders prepared by spray pyrolysis at 1000 °C. Spherical dense V_2O_5 powders were prepared directly by spray pyrolysis at temperatures above the

melting point of V_2O_5. Some rodlike crystals formed during the quenching of the melted powders were converted into nanosized particles on the surface of the submicrometer-sized powders.

Figures 2 and 3 show the morphologies, dot-mapping images, and the energy-dispersive X-ray (EDX) line scans of the cross sections of the V_2O_5 powders with 7 and 15 wt % ZrO_2, respectively. The powders with 7 wt % ZrO_2 were completely spherical and dense with a clean surface, on which the crystals of pure V_2O_5 powders were scarcely observed. The mean size of the powder with 7 wt % ZrO_2, as measured from the SEM images, was 0.78 μm. In the spray pyrolysis process, the size of each particle was dependent on the size of the droplet from which it formed because one particle was formed by drying and decomposing one droplet. Therefore, the sizes of the particles were uniformly distributed could be prepared using spray pyrolysis with a well-established atomizer or by introducing a droplet classifier between the droplet generator and the tubular furnace reactor to increase the sharpness of the size distribution of the particles. The dot-mapping images and EDX line scans of the V_2O_5 powders with 7 wt % ZrO_2 show that the V and Zr components are uniformly distributed inside the powders (Figure 2c and 2d). However, when the Zr component is uniformly distributed inside the powders, the crystallization of V_2O_5 is disturbed during the quenching of the melted powders. On the other hand, the TEM image, dot-mapping images, and the results of EDX line scan show that well-faceted crystals with a cubic structure are located at the center of the V_2O_5 powders with 15 wt % ZrO_2 (Figure 3b–d). The Zr component segregated to afford single-crystalline powder even when the residence time of the powders inside the hot wall reactor was as short as 2.2 s. The melted V_2O_5 acted as the flux to form single-crystalline ZrO_2 at a preparation temperature of 1000 °C. Rod-like crystals of V_2O_5 were observed both inside and on the surface of the powders with 15 wt % ZrO_2 in the TEM and dot-mapping images (shown by arrows in Figure 3b). Segregation of the Zr component did not disturb the crystallization of V_2O_5 during the quenching of the powders. When 7 wt % ZrO_2 was added, the V and Zr components were uniformly distributed inside the powder because the amount of Zr atoms was insufficient for crystal growth. However, when the added amount of ZrO_2 was increased to 15 wt %, Zr-based crystals were formed inside the spherical powder. The real ZrO_2 content of the prepared powders as shown in Figures 2 and 3 analyzed by ICP method were 7.2 and 14.4 wt %. The composition of the spray solution was well-maintained in the prepared powders.

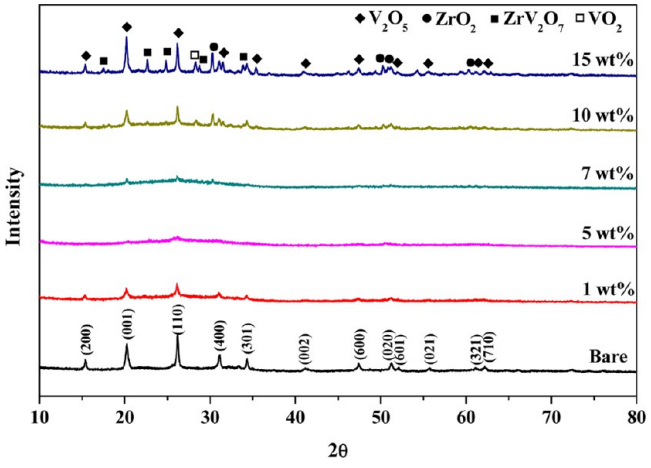

Figure 4. XRD patterns of the V_2O_5 powders prepared by spray pyrolysis with various ZrO_2 contents.

Figure 4 shows the crystal structures of V_2O_5 powders with various amounts of ZrO_2 additive. The XRD pattern of the powders without the ZrO_2 additive corresponded with the orthorhombic structure of V_2O_5 (JCPDS 41–1426), and no impurity phases were observed from the pattern. However, the XRD pattern of the pure V_2O_5 powders had low peak intensities because of the poor crystallinity. As seen in the TEM image in Figure 1, the complete crystallization of V_2O_5 powders did not occur during the quenching of the melted powders. Small amounts of ZrO_2 (below 7 wt % of the powders) suppressed the crystal growth of V_2O_5 during the quenching process. The V_2O_5 powders with 5 and 7 wt % ZrO_2 were amorphous, and small crystalline peaks of V_2O_5 could be seen in the XRD spectra. In contrast, the XRD patterns of V_2O_5 powders with 10 and 15 wt % ZrO_2 showed that the main crystal structure comprised the V_2O_5 phase, while the impurity peaks were due to VO_2, ZrO_2, and ZrV_2O_7. Crystal growth of ZrO_2 and ZrV_2O_7 through the assembly of the Zr component occurred inside the V_2O_5 powders with a ZrO_2 content of above 10 wt %. Figure 5 shows the V 2p XPS spectra of the powders with 7 and 15 wt % ZrO_2. In the V_2O_5 powders with 7 wt % ZrO_2, vanadium existed most commonly as V^{5+} oxidation states with scantly V^{4+} ions. This result indicated that the amorphous compound with 7 wt % ZrO_2 was identified to V_2O_5. Large amount of ZrO_2 additive of 15 wt % occupied the VO_2 impurity as shown in the XRD spectrum in Figure 4, so the low valence vanadium ions were identified in the V 2p XPS spectrum. The V $2p_{3/2}$ spectrum

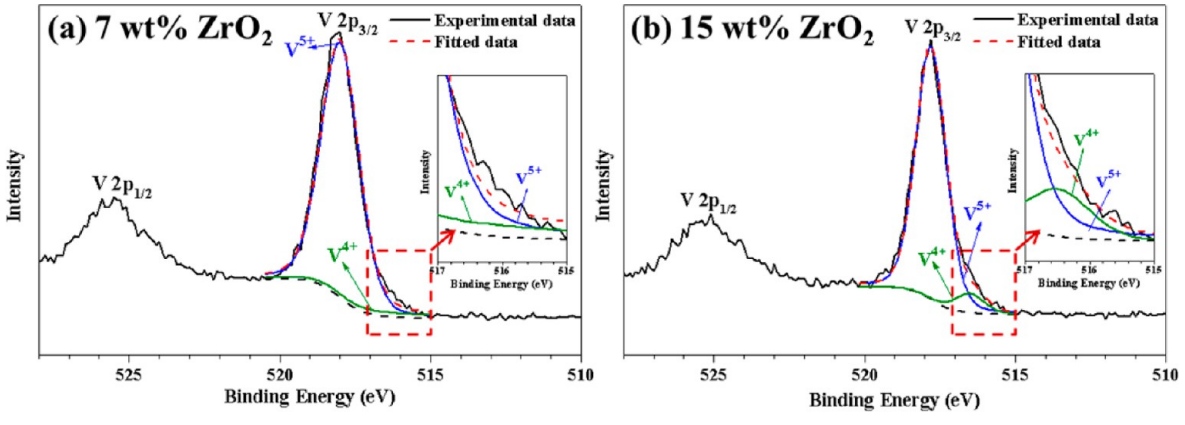

Figure 5. V 2p XPS spectra of the V_2O_5 powders with 7 and 15 wt % ZrO_2.

dx.doi.org/10.1021/am303150v | ACS Appl. Mater. Interfaces 2013, 5, 3234–3240

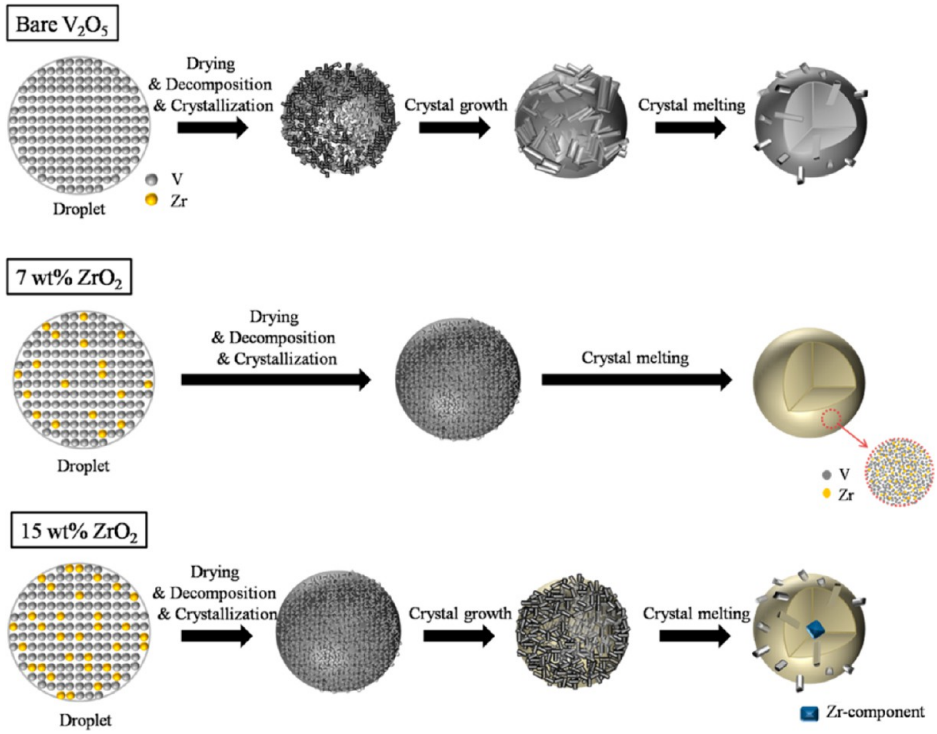

Figure 6. Formation mechanisms of the V_2O_5 powders with various amount of ZrO_2 additives.

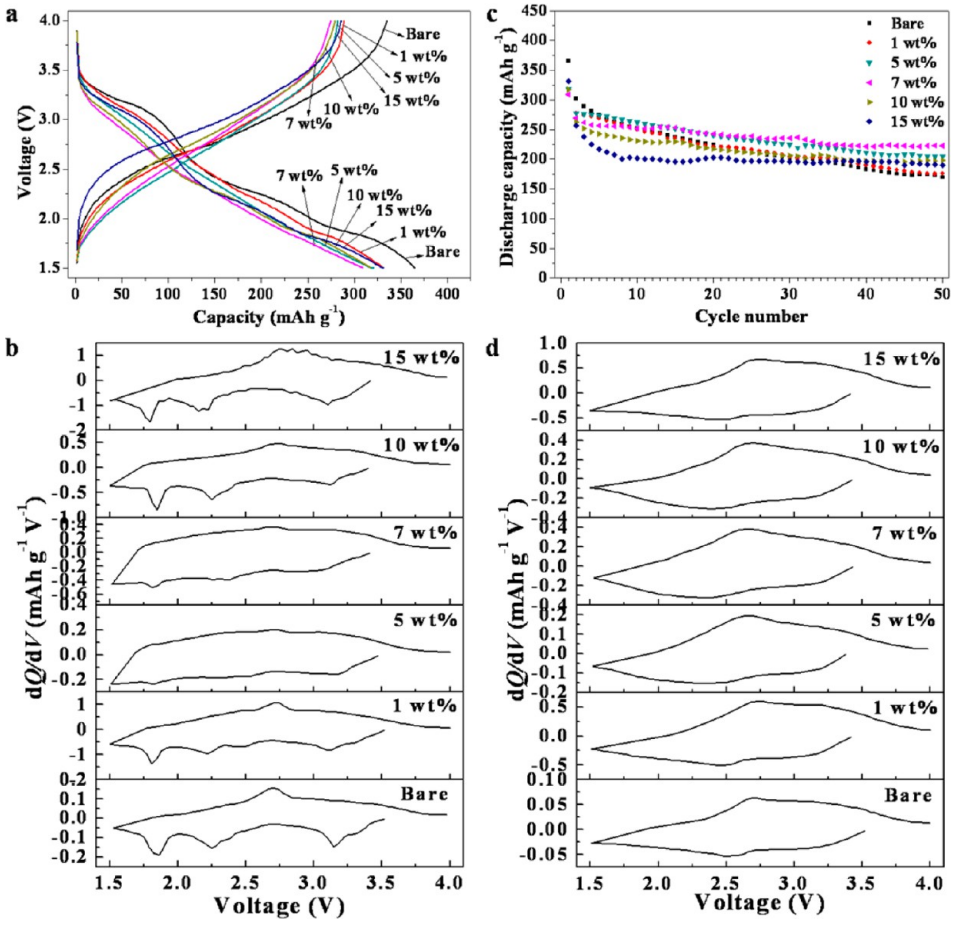

Figure 7. Electrochemical properties of the V_2O_5 powders with various amount of ZrO_2 additives at a constant current density of 294 mA g^{-1}. (a) Initial charge/discharge curves, (b) first incremental capacity curves (dQ/dV), (c) cycle properties, and (d) 50th incremental capacity curves (dQ/dV).

dx.doi.org/10.1021/am303150v | ACS Appl. Mater. Interfaces 2013, 5, 3234−3240

showed both V^{4+} and V^{5+} ions coexist in the V_2O_5 powders with 15 wt % ZrO_2.

Figure 6 describes the formation mechanisms of the V_2O_5 powders for various amounts of ZrO_2 additive. V_2O_5–ZrO_2 composite powders with a uniform composition were formed by fast drying and decomposition of the droplets containing the V and Zr components, regardless of the amount of additive. ZrO_2 when present in small amount (7 wt %) disturbed the crystallization of the melted V_2O_5 powders. Segregation of the Zr component did not occur inside the composite powders when the amount of ZrO_2 additive was below 7 wt %. However, when the amount of ZrO_2 was too high as 15 wt %, the Zr component segregated to form ZrO_2 and ZrV_2O_7 crystals. The segregation of ZrO_2 inside the powders determined the crystallization of the V_2O_5 phase of the composite powders during the quenching of the melted V_2O_5.

The electrochemical performance of V_2O_5 powders with various amounts of ZrO_2 additive was investigated in the 1.5–4 V range at a constant current density of 294 mA g^{-1}. The electrochemical properties of the powders prepared by spray pyrolysis from the aqueous spray solution showed high reproducibility because of their uniform composition with few impurities. In this study, the measurements were carried out three times at each sample and good reproducibility was indicated except negligible changing of the capacities. Figure 7a shows the initial charge/discharge curves. The initial discharge curve of the crystalline V_2O_5 powders had four distinct plateaus attributable to the phase transitions between α-$Li_xV_2O_5$ ($x < 0.01$), ε-$Li_xV_2O_5$ ($0.35 < x < 0.7$), δ-$Li_xV_2O_5$ ($x = 1$), γ-$Li_xV_2O_5$ ($1 < x < 2$), and ω-$Li_xV_2O_5$ ($2 < x \leq 3$).[4,28] However, V_2O_5 powders with 5 and 7 wt % ZrO_2 showed smooth initial discharge curves with a single slope a typical property of amorphous materials. The amorphous V_2O_5 film formed by cosputtering, too, did not show plateaus corresponding to the phase transitions of $Li_xV_2O_5$.[29] However, partially crystallized V_2O_5 powders with 0, 10, and 15 wt % ZrO_2 had four small plateaus in their initial discharge curves. Figure 7b shows the differential capacity vs voltage (dQ/dV) curves for the first cycles. The bare V_2O_5 powders had the distinct cathodic peaks at 3.32, 3.14, 2.25, and 1.86 V, and anodic peak at around 2.7 V in the dQ/dV curve which related to the formation of ε-$Li_xV_2O_5$, δ-$Li_xV_2O_5$, γ-$Li_xV_2O_5$, and ω-$Li_xV_2O_5$ phases, respectively. Depending on the ZrO_2 content, the cathodic and anodic peaks of the first dQ/dV curves changed. The amorphous V_2O_5 powders with 5 and 7 wt % ZrO_2 gave no evident cathodic and anodic peaks in their dQ/dV curves. The V_2O_5 powders with 0, 1, 5, 7, 10, and 15 wt % ZrO_2 showed initial discharge capacities of 365, 332, 319, 309, 318, and 331 mA h g^{-1}, respectively. Figure 7c shows the cycle performance of V_2O_5 powders with various amounts of ZrO_2. Regardless of the amount of the additive, the V_2O_5 powders showed large first irreversible capacity losses, which resulted from the formation of the irreversible phase. Once the irreversible ω-$Li_xV_2O_5$ phase is formed during the initial lithiation process, Li ions cannot be completely removed during the initial delithiation process.[28,30] After 50 cycles, the discharge capacities of the V_2O_5 powders with 0, 1, 5, 7, 10, and 15 wt % ZrO_2 decreased to 169, 176, 205, 222, 198, and 190 mA h g^{-1}, and the corresponding capacity retentions measured after the first cycles were 56, 63, 74, 83, 75, and 74 %, respectively. The crystalline V_2O_5 powders had relatively higher initial discharge capacities than did those with amorphous V_2O_5. However, crystalline V_2O_5 powders suffer from poor cycle performance because of the damage caused to the crystal structures during cycling. In contrast, amorphous V_2O_5 powders with the appropriate amount of ZrO_2 additive showed good cycle performance even at a high current density of 294 mA g^{-1} because of the faster Li ion diffusion. After the 50th cycle, only single broad cathodic and anodic peaks occurred at ~2.5 and 2.7 V in the dQ/dV curves (Figure 7d), which indicated the irreversible phase transformation during the cycling. The dQ/dV curves of the crystalline V_2O_5 changed into smooth ones, as in the case of the amorphous V_2O_5 after 50 cycles.

Figure 8 shows the surfaces of the V_2O_5 electrodes after cycling. The cracks were observed in the partially crystallized

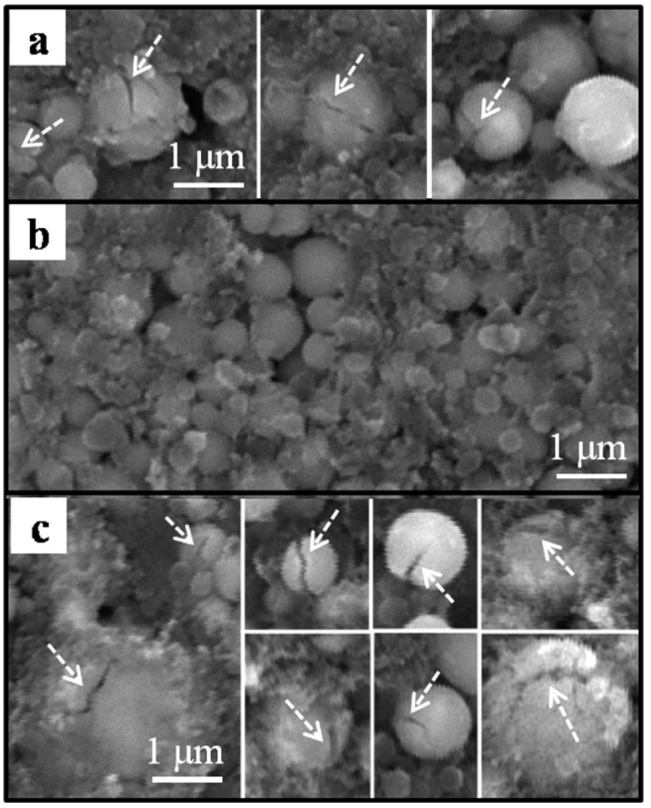

Figure 8. SEM images of the V_2O_5 electrodes after cycling. (a) Bare V_2O_5; (b) V_2O_5 with 7 wt % ZrO_2; (c) V_2O_5 with 15 wt % ZrO_2.

V_2O_5 powders with 0 and 15 wt % ZrO_2 as shown by arrows in Figure 8a and 8c. The formation of the cracks, which is one of the reasons of the capacity fading, is due to the volume expansion of electrode during cycling. However, the amorphous V_2O_5 powders with 7 wt % ZrO_2 maintained the spherical and dense morphologies after electrochemical test (Figure 8b). Thus, the amorphous V_2O_5 powders with the appropriate amount of ZrO_2 additive had good electrochemical properties. Zirconium dopant also improved the electrochemical properties of the amorphous V_2O_5 powders by act as a structural pinpoint to main the original structure during cycling process.[31]

4. CONCLUSIONS

The effect of ZrO_2 dopant on the crystal structure, morphology, and electrochemical performance of V_2O_5 cathode powders directly prepared by spray pyrolysis were investigated. The zirconia dopant played a key role in the formation of spherical, fine-sized amorphous V_2O_5 powders. The presence of a small amount of ZrO_2 additive disturbed the crystallization of the melted V_2O_5 powders during the quenching process.

Crystalline V_2O_5 powders showed relatively high initial discharge capacities than did the amorphous V_2O_5. However, crystalline V_2O_5 powders showed poor cycle performance because of the damage caused to the crystal structures during cycling. In contrast, the amorphous V_2O_5 powders with the appropriate amount of ZrO_2 additive exhibited good cycle performance even at a high current density of 294 mA g^{-1}.

AUTHOR INFORMATION

Corresponding Author

*Tel: +82-2-2049-6010. Fax: +82-2-458-3504. E-mail: yckang@konkuk.ac.kr.

Notes

The authors declare no competing financial interest.

ACKNOWLEDGMENTS

This work was supported by the National Research Foundation of Korea (NRF) grant funded by the Korea government (MEST) (2012R1A2A2A02046367).

REFERENCES

(1) Cao, A. M.; Hu, J. S.; Liang, H. P.; Wan, L. J. *Angew. Chem., Int. Ed.* **2005**, *44*, 4391−4395.

(2) Pan, A.; Wu, H. B.; Zhu, T.; Lou, X. W. *ACS Appl. Mater. Interfaces* **2012**, *4*, 3874−3879.

(3) Yu, D.; Chen, C.; Xie, S.; Liu, Y.; Park, K.; Zhou, X.; Zhang, Q.; Li, J.; Cao, G. *Energy Environ. Sci.* **2011**, *4*, 858−861.

(4) Ng, S. H.; Chew, S. Y.; Wang, J.; Wexler, D.; Toumayre, Y.; Konstantinov, K.; Liu, H. K. *J. Power Sources* **2007**, *174*, 1032−1035.

(5) Ponzio, E. A.; Benedetti, T. M.; Torresi, R. M. *Electrochim. Acta* **2007**, *52*, 4419−4427.

(6) Chernova, N. A.; Roppolo, M.; Dillon, A. C.; Whittingham, M. S. *J. Mater. Chem.* **2009**, *19*, 2526−2552.

(7) Wang, Y.; Takahashi, K.; Lee, K.; Cao, G. Z. *Adv. Funct. Mater.* **2006**, *16*, 1133−1144.

(8) Zhai, T.; Liu, H.; Li, H.; Fang, X.; Liao, N.; Li, L.; Zhou, H.; Koide, Y.; Bando, Y.; Golberg, D. *Adv. Mater.* **2010**, *22*, 2547−2552.

(9) Li, X.; Li, W.; Ma, H.; Chen, J. *J. Electrochem. Soc.* **2007**, *154*, A39−A42.

(10) Pan, A.; Zhang, J. G.; Nie, Z.; Cao, G.; Arey, B. W.; Li, G.; Liang, S. Q.; Liu, J. *J. Mater. Chem.* **2010**, *20*, 9193−9199.

(11) Chou, S. L.; Wang, J. Z.; Sun, J. Z.; Wexler, D.; Forsyth, M.; Liu, H. K.; MacFarlane, D. R.; Dou, S. X. *Chem. Mater.* **2008**, *20*, 7044−7051.

(12) Sudang, G.; Baudrin, E.; Dunn, B.; Tarascon, J. M. *J. Electrochem. Soc.* **2004**, *151*, A666−A671.

(13) Baudrin, E.; Sudant, G.; Larcher, D.; Dunn, B.; Tarascon, J. M. *Chem. Mater.* **2006**, *18*, 4369−4374.

(14) Cohem, Y. S.; Aurbach, D. *Electrochem. Commun.* **2004**, *6*, 536−542.

(15) Aurbach, D.; Markovsky, B.; Salitra, G.; Markevich, E.; Talyossef, Y.; Koltypin, M.; Nazar, L.; Ellis, B.; Kovacheva, D. *J. Power Sources* **2007**, *165*, 491−499.

(16) Patoux, S.; Wurm, C.; Morcrette, M.; Rousse, G.; Masquelier, C. *J. Power Sources* **2003**, *278*, 119−121.

(17) Chan, C. K.; Peng, H. L.; Twesten, R. D.; Jarausch, K.; Zhang, X. F.; Cui, Y. *Nano Lett.* **2007**, *7*, 490−495.

(18) Wang, Y.; Takahashi, K.; Shang, H. M.; Cao, G. Z. *J. Phys. Chem. B* **2005**, *109*, 3085−3088.

(19) Owens, B. B.; Passerini, S.; Smyrl, W. H. *Electrochim. Acta* **1999**, *45*, 215−224.

(20) Park, H. K.; Smyrl, W. H.; Ward, M. D. *J. Electrochem. Soc.* **1995**, *142*, 1068−1073.

(21) McGraw, J. M.; Bahn, C. S.; Parilla, P. A.; Perkins, J. D.; Readey, D. W.; Ginley, D. S. *Electrochim. Acta* **1999**, *45*, 187−196.

(22) Scarminio, J.; Talledo, A.; Andersson, A. A.; Passerini, S.; Decker, F. *Electrochim. Acta* **1993**, *38*, 1637−1642.

(23) Kim, T. A.; Kim, J. H.; Kim, M. G.; Oh, S. M. *J. Electrochem. Soc.* **2003**, *150*, A985−A989.

(24) Coustier, F.; Passerini, S.; Smyrl, W. H. *J. Electrochem. Soc.* **1998**, *145*, L73−L74.

(25) Lee, S. H.; Cheong, H. M.; Liu, P.; Tracy, C. E. *Electrochem. Solid-State Lett.* **2003**, *6*, A102−A105.

(26) Feng, C. Q.; Wang, S. Y.; Zeng, R.; Guo, Z. P.; Konstantinov, K.; Liu, H. K. *J. Power Sources* **2008**, *184*, 485−488.

(27) Ko, Y. N.; Kim, J. H.; Choi, S. H.; Kang, Y. C. *J. Power Sources* **2012**, *211*, 84−91.

(28) Chen, Y.; Liu, H.; Ye, W. L. *Scripta Mater.* **2008**, *59*, 372−375.

(29) Kim, H. K.; Seong, T. Y.; Yoon, Y. S. *J. Power Sources* **2002**, *112*, 67−75.

(30) Chan, C. K.; Peng, H.; Twesten, R. D.; Jarausch, K.; Zhang, X. F.; Cui, Y. *Nano Lett.* **2007**, *7*, 490−495.

(31) Ren, X.; Hu, S.; Shi, C.; Zhang, P.; Yuan, Q.; Liu, J. *J. Solid State Ionics* **2012**, *16*, 2135−2141.